Droplet splashing on a thin liquid film

Christophe Josserand and Stéphane Zaleski
josseran@lmm.jussieu.fr || zaleski@lmm.jussieu.fr

Laboratoire de Modélisation en Mécanique,
CNRS and Université Pierre et Marie Curie (Paris VI)
8 rue du Capitaine Scott, 75015 Paris, France,

Abstract

We propose a theory predicting the transition between splashing and deposition for impacting drops. This theory agrees with current experimental observations and is supported by numerical simulations. It assumes that the width of the ejected liquid sheet during impact is precisely controlled by a viscous length l_ν. Numerous predictions follow this theory and they compare well with recent experiments reported by S.T. Thoroddsen (The ejecta sheet generated by the impact of a drop, J. Fluid Mech **451**, pp 373 (2002)).

1 Introduction

A raindrop splashing on the ground, the impact of a fuel droplet on the walls of a combustion chamber, pesticides sprays, ink-jet printing, all involve the same complex dynamics. These impacts arise in many different contexts, and have important industrial applications as well as relevance to the natural sciences, such as soil erosion. Photographs of splashing droplets, starting with Edgerton's classic[2], have become media icons. Splashing can occur at widely different scales, from the astronomical when a comet impacts a planet to the microscopic in laboratory experiments. Since the pioneering work of Worthington[3], many experimental, theoretical, and numerical works have been performed. Nevertheless the problem is far from being fully understood (for a review see [4], [5], [6]).

The present study concentrates on the early times of droplet impact on a thin preexisting liquid layer. The two principal outcomes are splashing and deposition. Splashing occurs for large Weber and Reynolds numbers and involves many different dynamics. In many cases, a thin liquid sheet jets almost immediately after the impact. It arises in a small "impact neck" region

located at radius r_K, at the intersection between the almost spherical drop and the upper boundary of the liquid layer. Starting at early times the sheet grows into a corolla and propagates radially from the drop. The end rim that grows at the edge of this corolla is unstable and developps fingers of liquid[7]. The fingers eventually break up into small droplets by the Rayleigh-Plateau instability. This whole process, shown on well-known photographs, has been described in numerous experimental papers (for instance see [1, 8, 9, 10]) and is generally called "corona" or "crown" splash. Such crown splash can still be produced until fairly low Weber and Reynolds number although it may not have enough time to break up and create secondary droplets. Also, usually at very high impact velocity or for impact on rough surfaces, the crown-type splash is not observed but a "prompt splash" is seen, in which secondary droplets are emitted immediately after the impact without any observable smooth sheet or corolla at the base. Below the velocities at which all these kinds of splashes are present, the drop only spreads gently on the surface without emitting jets nor secondary droplets.

An empirical relation has been established experimentally for the cross-over between spreading and deposition behaviors through the dimensionless "Sommerfeld parameter" $K = \mathrm{We}^{\frac{1}{2}}\mathrm{Re}^{\frac{1}{4}}$, where We is the Weber number and Re the Reynolds number (as defined below)[9, 11, 12]. When K is smaller than a threshold value K_c then only deposition is observed, while for $K > K_c$ a splash develops. A reasonable estimate is $K_c \sim 50$ although the exact value of K_c depends on the roughness of the solid surface and on the thickness of the liquid layer.

Direct numerical simulations for drops impacting on liquid layers are a relatively new topic. It has attracted the attention of many researchers [13, 14, 15, 16, 17] but only recently. Several of the simulations are based on a potential flow model with surface tension in axisymmetric geometry. They exhibit corolla formation and the $r_K \sim t^1 2$ spreading law [13, 15, 16]. In particular, simulations have shown that for strong impacts (large Weber numbers) a jet was formed in the neck region defined as the region of the interface where the drop and the film meet[15, 16]. However, potential flow calculations cannot exhibit the effect of viscosity while the Sommerfeld law includes it to predict the splashing-deposition transition. The theory that follows indeed shows why. Our theory investigates the splash dynamics with special emphasis on jet formation at short times.

In simulations, we included viscosity and surface tension and solved the Navier-Stokes equations with sharp interfaces between a liquid and a gas phase. Momentum balance was solved on a very fine square grid. Interface tracking and conditions on the interface use Volume of Fluid (VOF) tracking as in [18, 19].

The theory below starts by assuming potential flow, which is then matched to a small viscous region at the impact neck.

2 Numerical Method

We consider a liquid drop of diameter D, density ρ_L and dynamic viscosity μ_L. It impacts at speed U onto a thin liquid layer of the same liquid of thickness h. The surrounding gas has density ρ_G and viscosity μ_G, the tension of the interface is σ. These initial conditions are shown on Figure 1.

We solve the axisymmetric incompressible Navier-Stokes equation with surface tension. Written in the one-fluid formulation, the equations read

$$\rho(\frac{\partial \mathbf{u}}{\partial t} + \mathbf{u} \cdot \nabla \mathbf{u}) = -\nabla p + \nabla \cdot (2\mu \mathbf{D}) + \sigma \kappa \delta_s \mathbf{n} \tag{1}$$

where $\mathbf{u} = (u, v)$ is the fluid velocity, ρ the fluid density, $\mathbf{D} = \frac{1}{2}\left(\nabla \mathbf{u} + (\nabla \mathbf{u})^{\mathbf{T}}\right)$ is the rate of deformation tensor and p is the pressure. $\mathbf{n}$ denotes the normal to the interface and δ_s is the bidimensional delta function restricted to the interface. The viscosity and density are constant in each phase. Gravity is neglected and the continuity equation is :

$$\nabla \cdot \mathbf{u} = 0 \tag{2}$$

Later on we will consider only axisymmetric dynamics. The discretization is performed on a Marker and Cell (MAC) grid and pressure is solved by the explicit projection method making use of multigrid convergence. The interface is followed by the Volume of Fluid/Piecewise Linear Interface Calculation (VOF/PLIC) method of [20] and the capillary force is computed through a variant of the continuous surface stress and continuous surface force methods [21, 19, 18] adapted to axisymmetric geometry. A full description of the method can be found in [18] except for the adaptation to axisymmetric geometry which is described in [22].

In this paper we investigate various grids from 128×128 to 512×512. We have found that 256×256 grid points are needed to obtain a fair description of the impact, although we sometimes perform control runs on the finest grid (512×512).

The VOF calculation is started with a droplet travelling at a prescribed velocity towards the fluid layer. At some time the two fluid regions reconnect. This involves various very small spatial scales. A thin gas layer forms between the two liquid regions and must be expelled. Under certain conditions voids or gas bubbles are actually entrapped during the impact because the thin

layer cannot retract fast enough[13, 23]. Molecular forces, acting on very small length,would also affect the motion of the interfaces in reality. These effects are below the grid scale and are not simulated. For the moment these very early times are beyond the scope of our study. However since the numerical method is based on the precise resolution of the momentum balance and the mass conservation equation, we argue that the situation just after reconnection offers a realistic starting point for the simulation run.

Here the Weber and Reynolds numbers for the liquid are

$$\mathrm{We} = \frac{\rho_L U^2 D}{\sigma}, \ \mathrm{Re} = \frac{\rho_L U D}{\mu_L}$$

Additional dimensionless numbers are the ratio h/D and the two numbers ρ_G/ρ_L and μ_G/μ_L describing the gas. The effects of the gas are not considered in any detail here, although they are present and add realism to the simulations. The characteristic time of impact is $\tau = D/U$. In the present study, we neglect compressibility and gravity. This implies that the Mach number $\mathrm{Ma} = U/c_s$ and Froude number $\mathrm{Fr} = gD/U^2$ are small. For instance, for the impact of a waterdrop of $D = 2$ mm from a height of one meter, we obtain $\mathrm{Ma} = 3 \cdot 10^{-3}$ and $\mathrm{Fr} = 10^{-3}$. At very short times and scales, it is clear that gravity has an even smaller effect, but compressibility could be relevant. However even there, Lesser and Field [24] have shown that compressibility plays no significant role at the velocities considered below.

3 Theory

We attempt to analyze the early instants of impact in the large Reynolds and Weber number regime, when the descending sphere, if it were unperturbed by the impact, would intersect the upper plane of the liquid layer at a point J at a small distance $r_J(t) \simeq (DUt)^{1/2}$ from the origin (Figure 2).

Our theory is based on the principle that at these early times, most of the liquid layer and the impacting drop are unperturbed. Thus there is an outer region (called region I) for $|\mathbf{r}| \gg r_J$ in which the velocity is nearly constant in the falling fluid (region Ia) so $\mathbf{u} \simeq -U\mathbf{e}_y$, and near zero in the liquid layer (region Ib). Region I matches to an inner region II where the flow is perturbed. We first investigate the potential flow problem of impact. The horizontal length scale for that flow is $r_J(t)$, while the vertical distance between the free surfaces is $r_J^2/D = Ut$. It is likely that multiple solutions of the free surface potential flow problem exist, as is the case in other problems of this type [25]. In particular we may distinguish between solutions with and without jet (Figure 3). The solution without jet is reminiscent of the solution

for the water entry of a wedge, which was found by conformal mapping techniques in [25]. It consists there to find a self-similar solution defined by a geometrical length equivalent to r_J. Similar problems have also been considered for free surface flows[26, 27].

The base of the jet is on the horizontal length scale at distance $r_K = Cr_J$ from the origin, where C is a numerical constant given by the full solution of the potential flow problem. This constant will be taken equal to 1 in what follows, and so will be other dimensionless constants, to avoid carrying on too many unknown numerical constants. The jet thickness must match the vertical length scale so $e_J = Ut$.

The velocity v_J of the jet may be obtained by a mass conservation argument. We assume that no mass radiates to or from infinity, an assumption that will be discussed below. Then the mass that comes from the impacting sphere per unit time is

$$q = \rho U \pi r_K^2 \tag{3}$$

which has to be equal to the mass flux through the jet

$$q \simeq 2\pi \rho r_K e_J v_J \tag{4}$$

thus

$$v_j \simeq (t/\tau)^{-1/2} U \tag{5}$$

where $\tau = D/U$.

When the jet starts forming it ends with a rim which tends to recede through surface tension effects. The receding or Taylor-Culick velocity [28, 29] is given by

$$v_C \simeq \left(\frac{2\sigma}{\rho e_J}\right)^{1/2} \tag{6}$$

for a sheet of thickness e_J thus

$$v_C \simeq (t/\tau)^{-1/2} U \mathrm{We}^{-1/2} \tag{7}$$

If $v_C < v_J$ the length of the jet increases, but is on the other hand $v_C > v_J$ the jet cannot form. Thus a necesssary condition for the formation of the jet is that the Weber number is large. In that case, potential flow theory predicts that the jet may form at any time after impact. It remains to be explained why a potential flow solution with jet is selected over a solution without jet. In particular one needs to explain how the jet can appear in the free surface potential flow. We just notice that in the solution without jet the acceleration of the free surface at point K in Figure 3 points from the gas to the liquid, which indicates that the interface is unstable with respect to the

Rayleigh-Taylor instability in the frame of reference moving with the fluid, and for two-dimensional perturbations. These perturbations would naturally lead to the formation of a jet. This inviscid theory with jet is supported by numerical simulations which show very early jet formation in high resolution runs.

If viscous effects are included we may find a viscous length scale of the order of $l_\nu \simeq (\nu t)^{1/2}$. This length scale is larger than the vertical length scale Ut of the potential solution for $t < t_\nu$ where $t_\nu = \tau \mathrm{Re}^{-1}$. It defines a region III at the base of the jet. Vorticity is also concentrated in region III. Indeed it is created in the highly curved regions of the interface at the base of the jet, then diffuses to distances of order l_ν. The solution in region III merges to the jet-like flow outside it. The analysis of the dynamics in this region presents a peculiar property since both viscous length l_ν and geometrical intersection r_J follow the same regime in square-root of the time. Thus the viscous effects appear has a self-similar correction embedded in the geometrical dynamics. The jet has naturally a thickness of the order of the size of region III $e_J = l_\nu$. When this happens the velocities of the jet and the receding tip are modified: the above argument now yields

$$v_J \simeq \mathrm{Re}^{1/2} U \tag{8}$$

while

$$v_C \simeq U(t/\tau)^{-1/4} \mathrm{We}^{-1/2} \mathrm{Re}^{1/4} \tag{9}$$

The condition $v_C < v_J$ for jet formation now implies

$$\mathrm{Re}^{1/2} \mathrm{We} \left(\frac{t}{\tau}\right)^{1/2} > 1 \tag{10}$$

This condition gives a time t_J after which the jet can form

$$t_J \simeq \tau K_c^4 \mathrm{Re}^{-1} \mathrm{We}^{-2} \tag{11}$$

This time is always shorter than t_ν for $\mathrm{We} \gg 1$ thus jet formation at t_J is consistent with the assumption of a viscous regime. Whenever t_J/τ is not small, the above may be seen as an approximation in the limit of large Re and We for the time of jet formation. Jet formation occurs early if $t_J < \tau$ that is when

$$\mathrm{We}^{1/2} \mathrm{Re}^{1/4} \leq K_c \tag{12}$$

We thus recover Sommerfeld's law.

Further predictions may be made if we assume a scaling form for the solution. For distances larger than l_ν the solution ought to be potential. For

$t > t_\nu$ this involves all length scales $\ell > Ut$, for $t < t_\nu$ the potential flow is limited to $\ell > l_\nu$. These conditions define region II, inside which we assume the scaling form for the velocity potential

$$\phi = UD(t/\tau)^n f(X, Y) \tag{13}$$

where X, Y are the rescaled variables $X = 1 - r/r_J$, $Y = z/r_J$, and n is an exponent to be determined. The potential must satisfy boundary conditions on a free surface. The free surface must be determined a part of the solution but asymptotes to the spherical surface of the drop at large distance from region II.

In region II the pressure also scales as

$$p = \rho U^2 (t/\tau)^m g(X, Y) \tag{14}$$

where g is another scaling function and m has to be determined. This may be done by a momentum conservation argument. To simplify the discussion we consider 2D flow and momentum per unit length in the third dimension. The downward momentum of the falling sphere is reduced by impact. This effect is felt in region II, so vertical momentum "lost" during the impact is of the order

$$M \simeq C\rho r_K^2 U \tag{15}$$

where C is a numerical constant of order 1 and the pressure increases this lost momentum by

$$\frac{dM}{dt} \simeq \int_0^{r_J} p dr \tag{16}$$

thus

$$\frac{1}{2}(DU/t)^{1/2} UC \simeq U^2 (t/\tau)^m \int_0^1 g(X, 0) dX \tag{17}$$

Assuming the integral converges, it is a constant term and we find $m = -1/2$. The maximum reached by the pressure depends on the behavior of g as $X \to 0$, $X = 0$ being the location of the base of the jet. Expression (14) is valid until the smallest length scale in region II is reached. For $t > t_\nu$ this length is Ut so $|X| \sim Ut/r_K = (t/\tau)^{1/2}$. Thus

$$p_{\max} \sim \rho U^2 (t/\tau)^{-1/2} g((t/\tau)^{1/2}, 0). \tag{18}$$

On the other hand when $t < t_\nu$ the minimum length is l_ν , $|X| \sim \mathrm{Re}^{-1/2}$ and

$$p_{\max} \sim \rho U^2 (t/\tau)^{-1/2} g(\mathrm{Re}^{-1/2}, 0). \tag{19}$$

On this basis it is possible to show that the pressure field is harmonic. The Bernouilli theorem for potential flow implies

$$\partial_t \phi + \frac{1}{2}(\nabla\phi)^2 + \frac{p}{\rho} = 0. \tag{20}$$

where the ∇ operator is in the original (unscaled) variables. We shall see that at short times the first and third term dominate the second. Balancing the third with the first term, we find that $n = 1/2$. The velocity may then be found by differentiating Equation (13) to yield

$$\nabla\phi = U\nabla_X f = U\mathbf{V}(\mathbf{X}, \mathbf{Y}) \tag{21}$$

where ∇_X is the gradient with respect to the scaled variables and $\mathbf{V}$ is a dimensionless function. Velocity is thus independent of time at first order, which is consistent with the need to match a constant velocity at X, Y large, as we go towards region I. Thus our hypothesis is confirmed, namely that the first and third terms of the Bernouilli equation, being of order $t^{-1/2}$ dominate the second. Thus

$$\partial_t \phi \simeq -\frac{p}{\rho}. \tag{22}$$

Since $\Delta\phi = 0$ we also must have

$$\Delta p = 0. \tag{23}$$

so the pressure field is harmonic as in the pressure-impulse theory. We retrieve here a property of the problem of pressure impact studied in [30].

4 Numerical results and discussion

For more insight into the splashing dynamics we now turn to the numerical simulation results. A series of simulations has been performed, for a 2-mm diameter droplet of a water-like liquid impacting a layer of the same liquid, 0.3 mm deep with a velocity of 10 $\mathrm{m{\cdot}s^{-1}}$. The gas is taken twice denser than air at atmospheric pressure ($\rho_L/\rho_g = 500$) and the surface tension has been taken a fraction of the air-water surface tension ($\sigma = 0.025$ $\mathrm{kg{\cdot}s^{-2}}$). The viscosity of the gas is taken slightly higher than for air ($\mu_g = 5{\cdot}10^{-4}\mathrm{kg{\cdot}m^{-1}{\cdot}s^{-1}}$). We only varied the viscosity of the liquid, from 0.02 to 0.5 $\mathrm{kg{\cdot}m^{-1}{\cdot}s^{-1}}$, with intermediate values 0.05, 0.1 and 0.2. The Weber number is thus 8000 for all cases while the Reynolds number evolves from 1000 to 40. The choice of these values was determined mainly by numerical stability and convenience to allow a large range of liquid Reynolds numbers. For

instance higher density ratios would lead to stronger numerical instability at the interface by spurious currents. Time $t = 0$ is set at the instant of impact. In addition, the liquid in the droplet and in the layer have been marked with two different colors, so that their specific evolution can be observed for various Reynolds numbers in Figures 4, 5 and 6.

These three simulations show important qualitative differences. The two less viscous impacts (figures 4 and 5) are splashing. The less viscous the fluid, the thinner the corolla and the larger the angle between the liquid sheet and the liquid layer. For the highest Reynolds number the impact is rapidly followed by secondary droplet break-up. Because of axisymmetry the liquid patches seen on figure 4 are actually toroidal. Further 3-D calculations would be needed to account properly for the evolution of the crown once non-axisymmetric perturbations grow[14, 31]. On the other hand, for $Re = 40$, the droplet spreads gently on the surface. The impact creates a radially expanding surface wave. Jet formation is visualized in Figure 7 a) where the interface profiles are shown near the neck of the impact as the jet is created, for $Re = 1000$.

The spreading radius r_K is detected automatically in the simulations. For this purpose it is defined as the radius of the point where the velocity of the fluid was maximal at a given instant. We have checked that this definition agrees with the visually determined spreading radius. In particular the basis of the corolla is well captured at large times and for high Reynolds number with this method. At short time this point almost coincides with the intersection between the drop and the liquid layer. Indeed we first observe that r_K and r_J follow the same scaling behavior:

$$r_K \simeq r_J(t) = \sqrt{DUt} \tag{24}$$

Actually, a more precise study gives $r_K = 1.1 \cdot r_J(t)$. It accounts thus for the mass conservation correction to the geometric law r_J. The theory above predicts a constant ratio r_K/l_ν with time. This is observed on figure 7 b) where the width of the jet is captured by two straight lines as r_K increases.

Figure 8 shows r_K for $We = 8000$ and $Re = 100$, 200, 400 and 1000. The geometric relation (24) is well verified for each curve and no significant dependence on the viscosity is found. We can remark that the geometric scaling law (24) is valid even at large times while the argument was only valid at short times. It is however a well established result for the impact radius[9, 32]. At larger times the dynamics of expansion is indeed imposed by an effective collision between the expanding liquid coming from the drop with the liquid of the layer at rest. It has been shown[9] that the dynamics is there controlled by a Burgers-type equation which leads to the same scaling (24).

There is here a remarkable coincidence: the physical principles that lead to the square-root behavior at short times are completely different from those leading to the scaling at long times. However in our range of simulations law (24) is valid with the same prefactor from short times to moderate times ($t/\tau \simeq 3$). No explanation has yet been found for this fact.

A pressure peak is observed in the simulation at the impact neck (Figure 9) as predicted in our theory. Figure 10 shows the maximum pressure in the liquid as a function of time for $We = 8000$ and $Re = 100$, 200, 400 and 1000. For these Reynolds numbers a jet is always created. The scale $\rho U^2 (t/\tau)^{1/2}$ is also shown on the figure and gives the corect behavior of the pressure peak for small time ($t/\tau < 1$). Indeed, for large Reynolds and small ratio t/τ the scaling (19) suggests that the pressure peak should follow this scale. However the dependence on $\mathrm{Re}^{1/2}$ does not appear here. The pressure drops rapidly as expected in our theory for $t \sim \tau$. The observation of the pressure field shows also that regions of equal pressure fan around the neck (see figure 9). Moreover, figure 11 exhibits the pressure profile near the neck at short times after the impact. The normalized pressure is exactly shown as a fonction of the normalized distance λ ($\lambda = |\mathbf{r} - r_K \mathbf{e_r}|/r_K$) along the vertical from the neck. The pressure drops spatialy from the impact center. The profiles however do not superpose, indicating that the asymptotic regime predicted by the theory has not yet been reached.

Eventually, we analyze the influence of viscosity on the vorticity field. The vorticity fields for $Re = 1000$ and $Re = 100$ are shown in Figure 12 for $t/\tau = 0.1$. It corresponds to the third snapshot of (4) and (5). The vorticity is concentrated near the neck and forms two counter-rotating vortex rings which expel the liquid towards the jet. Figure 13 a) follows the absolute mean amplitude of the vortex dipole as a function of time for the different Reynolds numbers explored already. The amplitude of the vortex dipole is computed through the difference between the highest (positive) and the lowest (negative) values of the vorticity in the liquid bulk. The four curves show a similar behavior but at different scale, and we observe that the larger the viscosity, the smaller the amplitude. The vorticity is indeed diffused through viscous diffusion over a distance $l_\nu(t)$ from the interface. Thus the vorticity scale should evolve like $1/\sqrt{Re}$ when viscosity varies. Actually, in figure 13 b) we present the same quantity rescaled by the factor $\sqrt{Re}$. We observe that all the curves converge to the same one, particularly at short times. This result validates the assumption of our theory that the length scale involved at the jet basis is selected by the viscous length l_ν.

There is little quantitative experimental data to compare our theory with. The scaling of the experimental law (12) is recovered with the critical number K_c estimated to be 225 in our numerics. Experimentally, K_c has been

found to vary between few tens and few hundreds, decreasing with the surface roughness. In our numerics, the surface has no roughness so that the observed K_c is consistent with experiments. Besides the Sommerfeld law there are few other experimental results with the exception of the recent work of Thoroddsen [1]. As in our theory, experiments show that the time at which the jet forms grows linearly with viscosity (equation 11). In addition the scaling law $v_J \sim \sqrt{ReU}$ (eq. 8) corresponds exactly to the measured dependance of the initial sheet velocity with viscosity reported in [1].

5 Conclusion

Our theory, supported by numerical simulations, predicts the scaling of the transition between splashing and deposition. It is in agreement with current experimental observations and in particular recovers the splashing-deposition criterion (12). Agreement is found with recent experimental observations such as the initial sheet velocity[1]. To summarize our theory, it constructs a potential flow everywhere except in a small neck region. Viscosity is shown to play a major role that region, selecting the width of the jet that develops into the crown. Surface tension then comes in to allow or prevent the formation of the jet.

Several points remain to be investigated in future experiments and simulations. A numerical investigation of the time of jet formation has not been possible, because the jet and the neck region that scales with it become too thin as the formation time recedes to zero.

However, one should remark a contradiction with results from calculations done with BIM methods [15]. There, a well-defined jet width is selected, while the asymptotic limit of our self-similar theory would suggest that a jet should be present at arbitrarily small times, with a vanishing thickness. It is possible that the BIM numerical method produces a short length scale cutoff there which limits the minimum size of the jet. This returns to the formation of a jet in a potential flow as pointed to above. A numerical confirmation of this hypothesis would clearly be interesting. In any case a physical cut-off of microscopic size will always be present in a real system. In our investigations the highest Reynolds number was actually restricted by the numerical cut-off of the finest jet width that could be resolved (here the thinest jet is 2 micrometers width). Further numerical developpements such as adaptive meshed refinement for instance would greatly improve this issue.

Another point of interest would be to investigate the shape of the emerging jet as it evolves into the corolla. This shape can be found by integration of the equations for a thin sheet with surface tension. Without surface tension

the problem is even simpler, as each sheet particle follows a ballistic path. The shapes depend on the angle of ejection of the jet (which our theory does not give). Moreover the location of the tip of the jet and the width of the associated rim depend on the time of appearance of the jet. Knowing the shape of the jet and the location of the end rim would allow to compute its stability with respect to perturbations, thus addressing the long-standing problem of crown formation. These unresolved issues regarding the shape of the interface and the angle of the jet could probably be resolved through a detailed analysis of potential flow in the neck region, which is the focus of ongoing investigations.

References

[1] S.T. Thoroddsen. The ejecta sheet generated by the impact of a drop. *J. Fluid Mech.*, 451:373, 2002.

[2] H.E. Edgerton and J.R. Killian. *Flash.* Boston: Branford, 1954.

[3] A.M. Worthington. On the form assumed by drops of liquids falling vertically on a horizontal plate. *Proc. R. Soc. Lond.*, 25:261–271, 1876.

[4] A. Prosperetti and H.N. Oğuz. The impact of drops on liquid surfaces and the underwater noise of rain. *Ann. Rev. Fluid Mech.*, 25:577, 1993.

[5] M. Rein. Phenomena of liquid drop impact on solid and liquid surfaces. *Fluid Dyn. Res.*, 12:61, 1993.

[6] R. Rioboo, M. Marengo, and C. Tropea. Outcomes from a drop impact on solid surfaces. *Atomization and Sprays*, 11:155–165, 2001.

[7] H.-Y. Kim, Z.C. Feng, and J.-H. Chun. Instability of a liquid jet emerging from a droplet upon collision with a solid surface. *Phys. Fluids*, 12:531–541, 2000.

[8] Z. Levin and P.V. Hobbs. Splashing of water drops on solid and wetted surface: hydrodynamics and charge separation. *Phil. Trans. R. Soc. Lond.*, 269A:555, 1971.

[9] A.L. Yarin and D.A. Weiss. Impact of drops on solid surfaces: self-similar capillary waves, and splashing as a new type of kinematic discontinuity. *J. Fluid Mech.*, 283:141–173, 1995.

[10] G.E. Cossali, A. Coghe, and M. Marengo. The impact of a single drop on a wetted solid surface. *Exps. Fluids*, 22:463–472, 1997.

[11] C.D. Stow and M.G. Hadfield. An experimental investigation of fluid flow resulting from the impact of a water drop with an unyielding dry surface. *Proc. R. Soc. London, Ser. A*, 373:419, 1981.

[12] C. Mundo, M. Sommerfeld, and C. Tropea. Droplet-wall collisions: Experimental studies of the deformation and breakup process. *Int. J. Multiphase Flow*, 21:151, 1995.

[13] H.N. Oğuz and A. Prosperetti. Bubble entrainment by the impact of drops on liquid surfaces. *J. Fluid Mech.*, 219:143–179, 1990.

[14] D. Gueyffier and S. Zaleski. Formation de digitations lors de l'impact d'une goutte sur un film liquide. *C. R. Acad. Sci. IIb*, 326:839–844, 1998.

[15] D.A. Weiss and A.L. Yarin. Single drop impact onto liquid films: neck distortion, jetting, tiny bubble entrainment, and crown formation. *J. Fluid Mech.*, 385:229–254, 1999.

[16] M.R. Davidson. Spreading of an inviscid drop impacting on a liquid film. *Chem. Eng. Sci. (to appear)*, 2001.

[17] M. Bussman, Chandra S., and J. Mostaghimi. Modeling the splash of a droplet impacting a solid surface. *Phys. Fluids*, 12:3121, 2000.

[18] D. Gueyffier, A. Nadim, J. Li, R. Scardovelli, and S. Zaleski. Volume of fluid interface tracking with smoothed surface stress methods for three-dimensional flows. *J. Comput. Phys.*, 152:423–456, 1999.

[19] R. Scardovelli and S. Zaleski. Direct numerical simulation of free-surface and interfacial flow. *Annu. Rev. Fluid Mech.*, 31:567–603, 1999.

[20] Jie Li. Calcul d'interface affine par morceaux (piecewise linear interface calculation). *C. R. Acad. Sci. Paris, série IIb, (Paris)*, 320:391–396, 1995.

[21] B. Lafaurie, C. Nardone, R. Scardovelli, S. Zaleski, and G. Zanetti. Modelling merging and fragmentation in multiphase flows with SURFER. *J. Comput. Phys.*, 113:134–147, 1994.

[22] D. Gueyffier. *Etude de l'impact de gouttes sur un film liquide mince.* PhD thesis, Université Pierre et Marie Curie, 2000.

[23] D. Duchemin, J. Eggers, and C. Josserand. Inviscid coalescence of drops. *Subb. to J. Fluid Mech.*, 2002.

[24] Lesser M.B.; and Field J.E. The impact of compressible liquids. *Annu. Rev. Fluid Mech.*, 15:97, 1983.

[25] P.R. Garabedian. Oblique water entry of a wedge. *Comm. Pure and Appl. Math.*, VI:157–165, 1953.

[26] J.B. Keller and M.J. Miksis. Surface tension driven flows. *SIAM J. Appl. Math.*, 43:268, 1983.

[27] M.J. Miksis and J.-M. Vanden-Broeck. Self-similar dynamics of a viscous wedge of fluid. *Phys. Fluids*, 11:3227–3231, 1999.

[28] G.I. Taylor. The dynamics of thin sheets of fluid iii. disintegration of fluid sheets. *Proc. Roy. Soc. London A*, 253:253–313, 1959.

[29] F.E.C. Culick. Comments on a ruptured soap film. *J. Appl. Phys.*, 31:1128, 1960.

[30] M.J. Cooker and D.H. Peregrine. Pressure-impulse theory for liquid impact problems. *J. Fluid Mech.*, 297:193–214, 1995.

[31] M. Rieber and A. Frohn. Numerical simulation of splashing drops. Academic Press, 6-8 July 1998. Proceedings of ILASS98, Manchester.

[32] Peregrine D.H. The fascination of fluid mechanics. *J. Fluid Mech.*, 106:59, 1981.

List of Figures

[Figure 1 about here.]

[Figure 2 about here.]

[Figure 3 about here.]

[Figure 4 about here.]

[Figure 5 about here.]

[Figure 6 about here.]

[Figure 7 about here.]

[Figure 8 about here.]

[Figure 9 about here.]

[Figure 10 about here.]

[Figure 11 about here.]

[Figure 12 about here.]

[Figure 13 about here.]

List of Figures

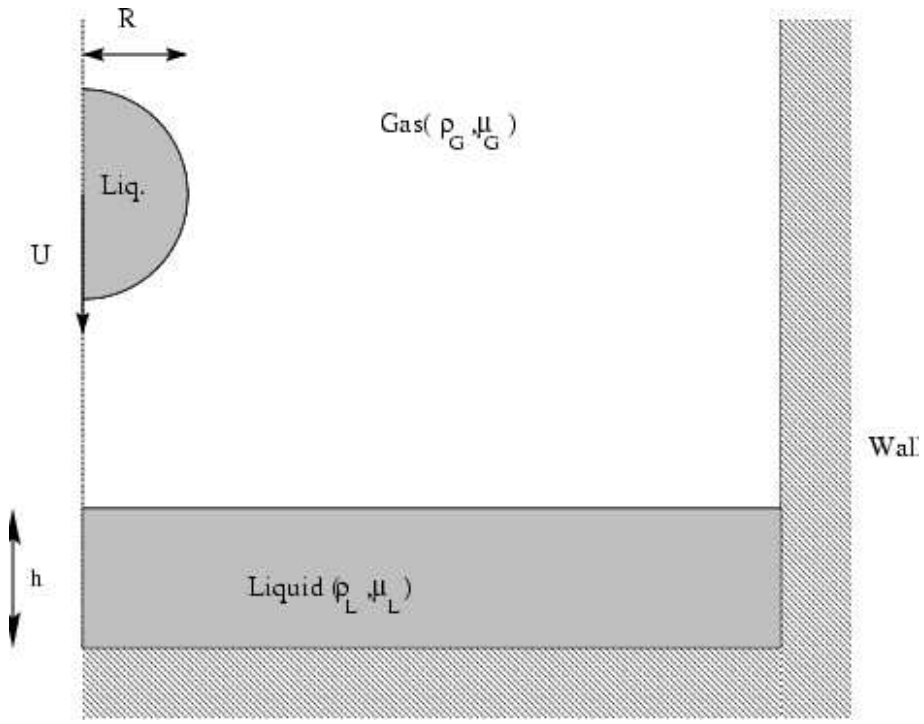

Figure 1: Representation of the simulation setup for the impact of a drop on a liquid layer.

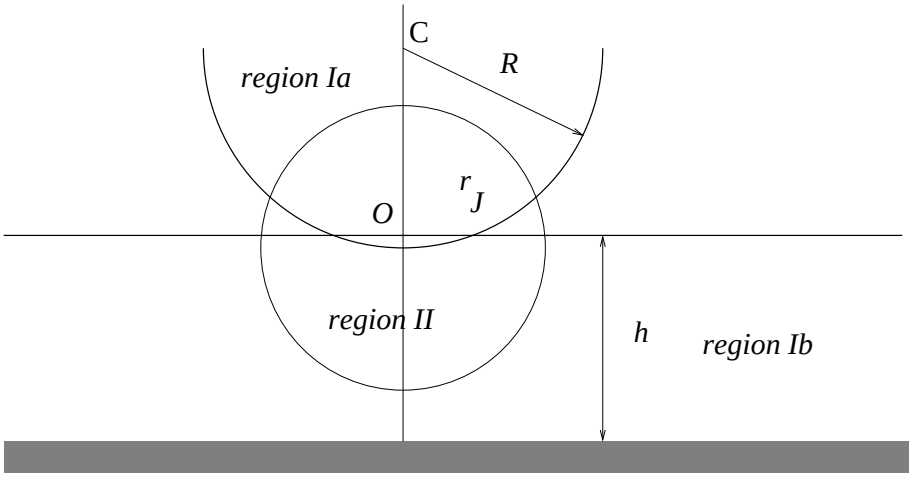

Figure 2: Geometry at early times. The unperturbed droplet and the unperturbed surface of the liquid layer intersect at distance r_J from the origin. The asymptotic analysis is performed by assuming the flow perturbed in region II only.

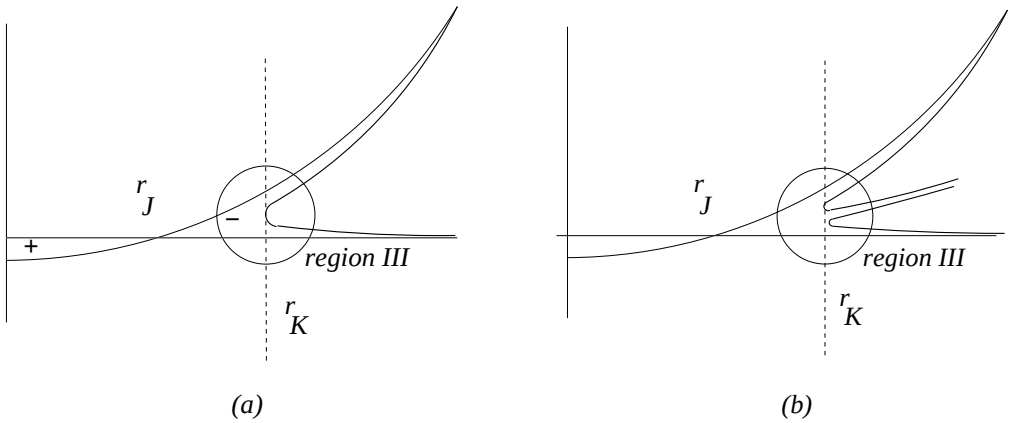

Figure 3: Two types of solution, without jet (a) and with jet (b). If mass does not flow in from, or oout to, infinity the areas marked + and − must be equal

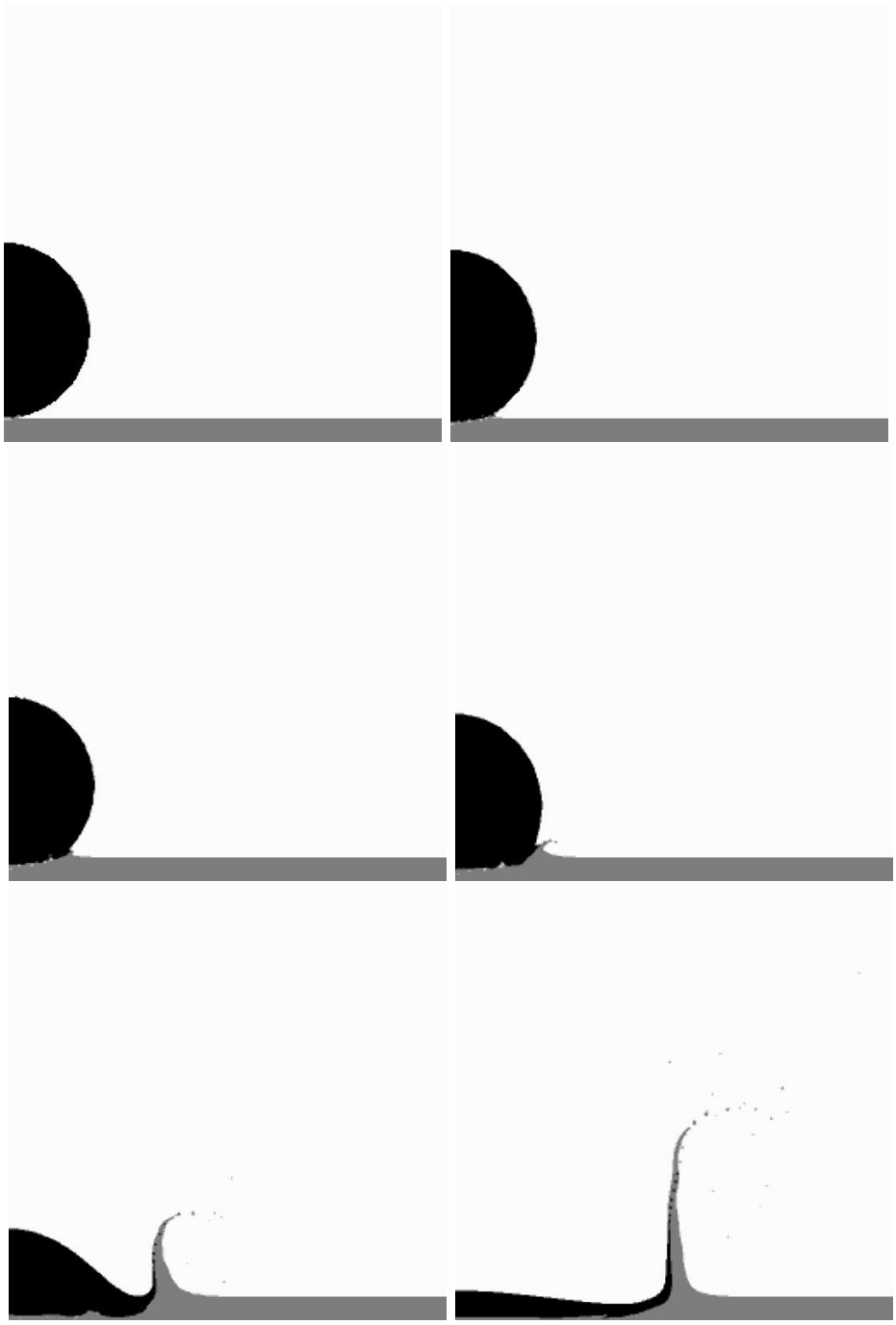

Figure 4: Density fields at $t = 0.01$ 0.05 0.1 0.2 0.7 and 1.5 unit time for $We = 8000$ and $Re = 1000$.

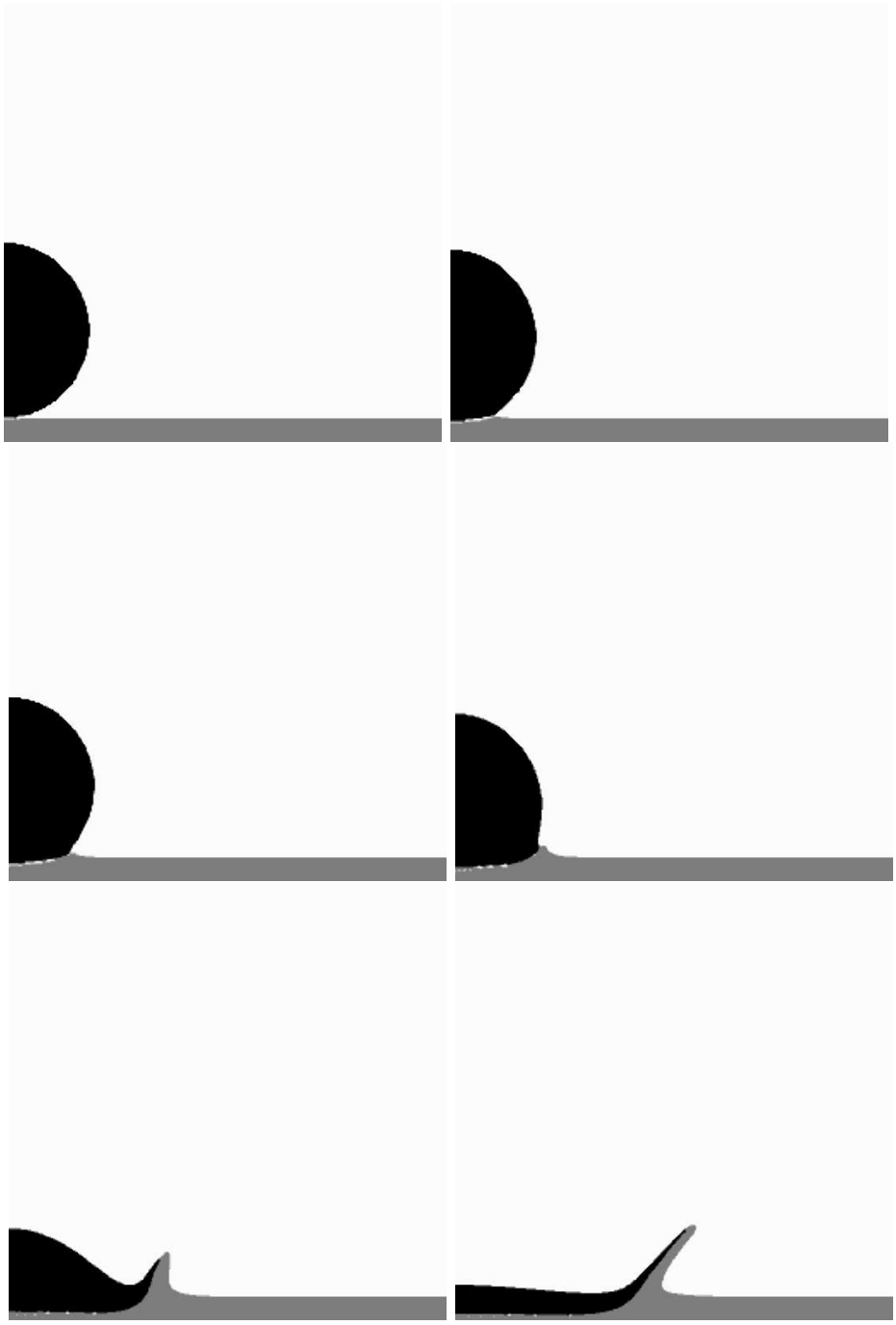

Figure 5: Density fields at $t = 0.01$ 0.05 0.1 0.2 0.7 and 1.5 unit time for $We = 8000$ and $Re = 100$

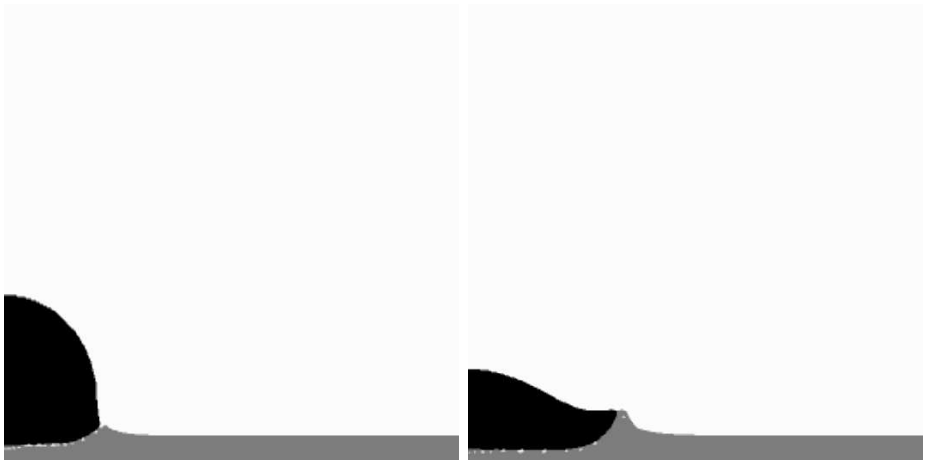

Figure 6: Density fields at $t = 0.5$ and $t = 1.5$ unit time for $We = 8000$ and $Re = 40$

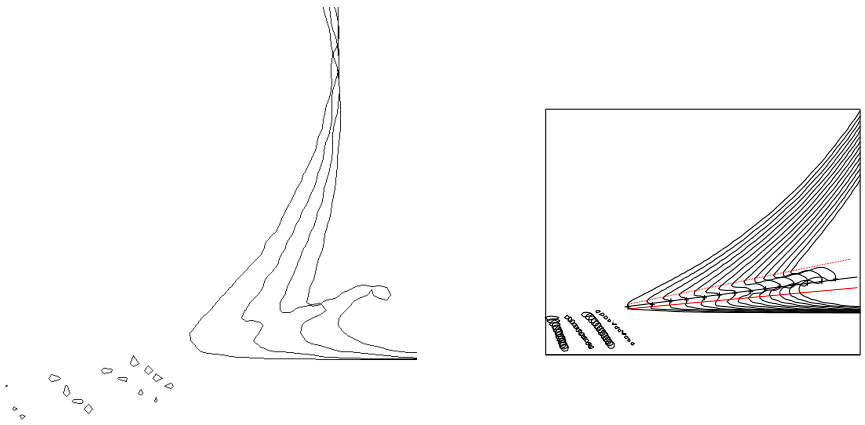

a) b)

Figure 7: a) Interface shapes near the neck of the impact, for $We = 8000$ and $Re = 1000$ (same case as figure (4)). The four profiles correspond to the times $t/\tau = 0.07$, 0.11, 0.15 and 0.19. We observe the formation of a jet coming out of the neck. The last profile shows the breakup of the jet. Numerically, it happens when the structure size is of the order of the grid size. b) The evolution of the jet width is contained by two straight dashed lines as the splash developps. The extremity of the jet is also followed by the straight solid line(courtesy of Denis Gueyffier [22]

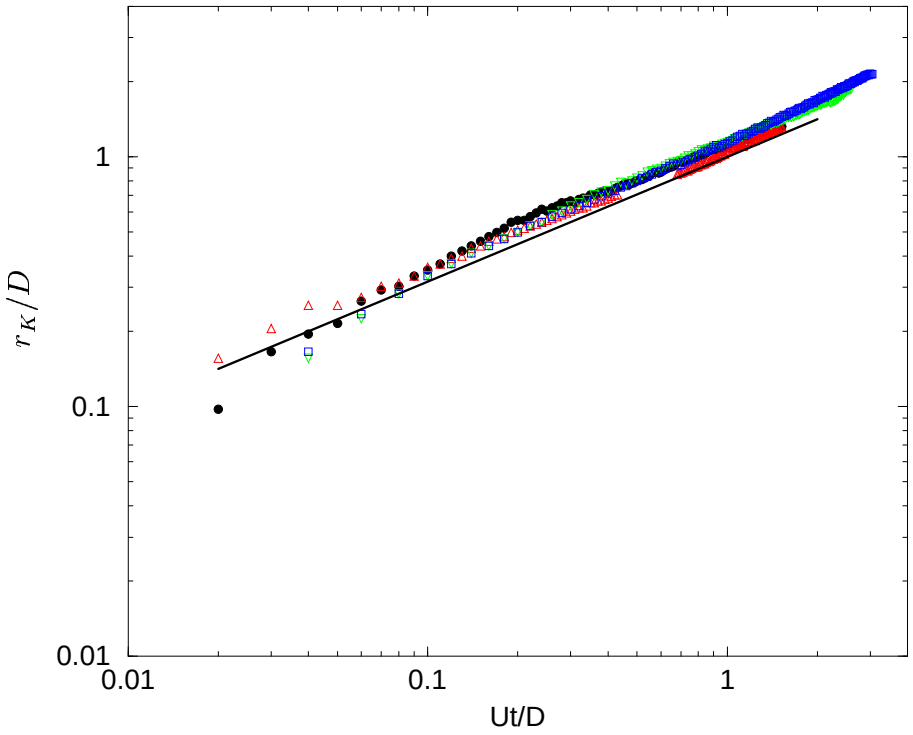

Figure 8: Log-log plot of the spread factor r/D as a function of Ut/D for the same Weber number (8000) and different Reynolds numbers (Re = 100, 200, 400 and 1000). The straight line corresponds precisely to the power law $r_J = \sqrt{DUt}$.

a) 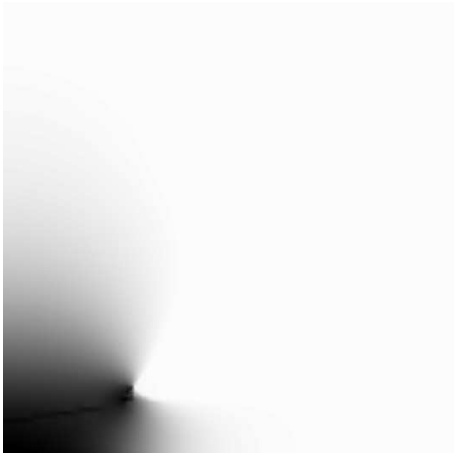 b) 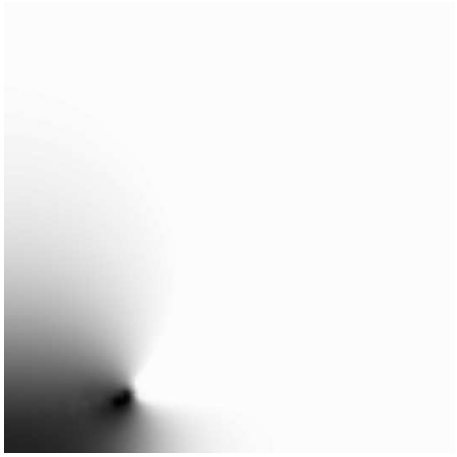

Figure 9: Pressure field near the neck of the impact for $t/\tau = 0.1$, $We = 8000$, and a) $Re = 100$ and b) $Re = 1000$. The color scale is the same for each figure, the higher the pressure the darker the color.

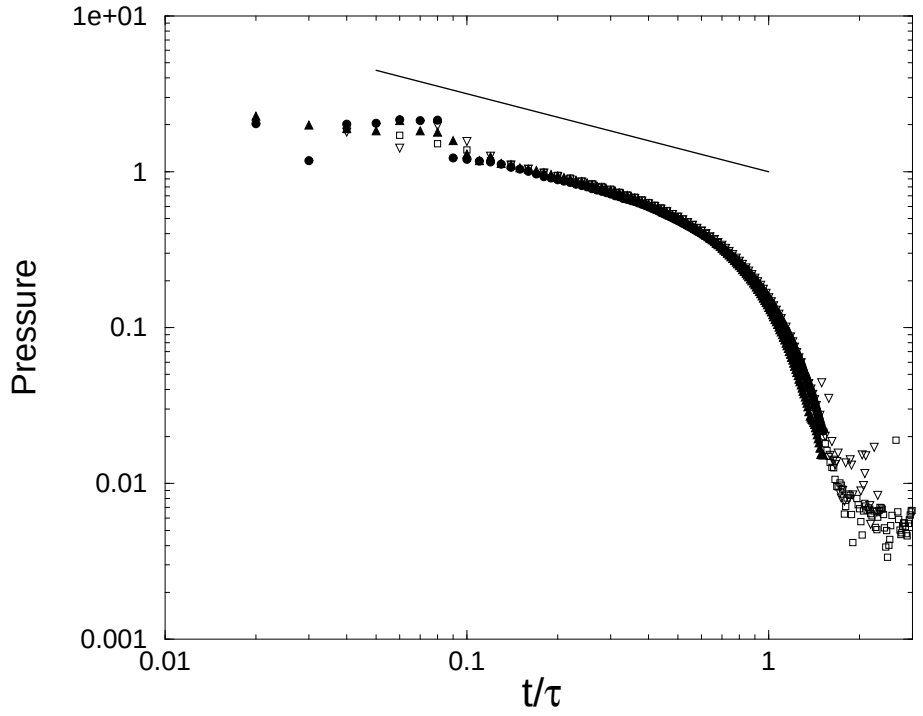

Figure 10: Log-log plot of the pressure peak P_{max} as a function of t/τ for the same Weber number (8000) and different Reynolds numbers (Re = 20, 100, 200, 400 and 1000). The pressure scale $\rho U^2 \left(t/\tau\right)^{1/2}$ is represented by the straight line above the curves.

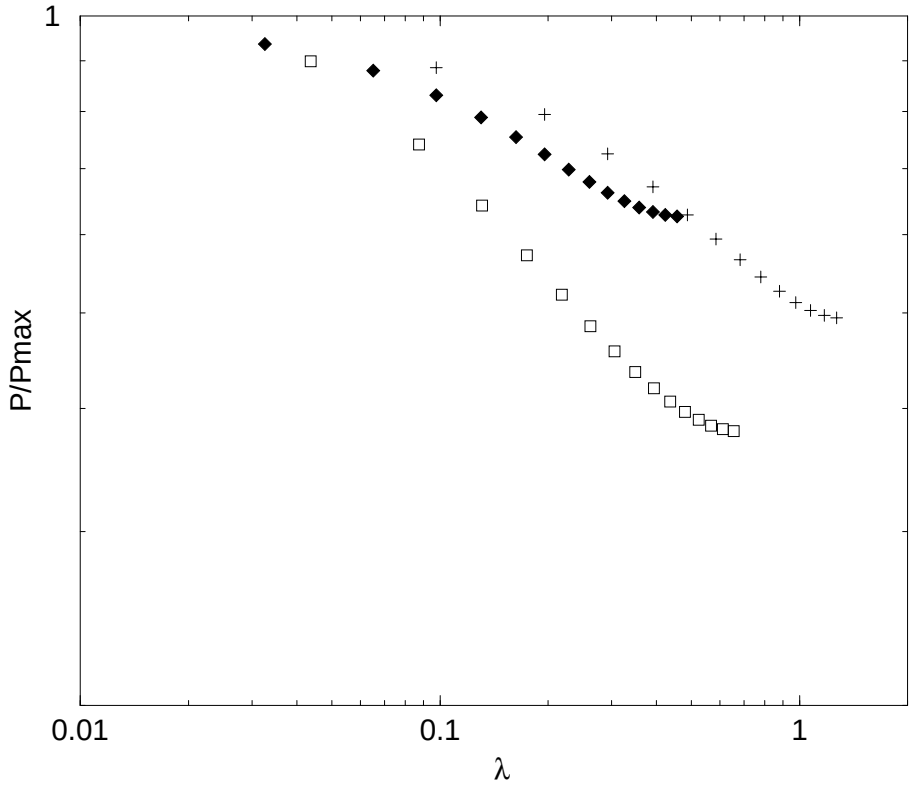

Figure 11: Pressure profiles from the neck center for $t/\tau = 0.01$ (circles) $t/\tau = 0.05$ (squares) and $t/\tau = 0.09$ (diamonds) for the less viscous case considered $Re = 1000$ and $We = 8000$. The pressure has been normalized by the pressure peak. The profiles are taken along the vertical direction from the neck and are shown as a function of λ the relative distance to the pressure peak.

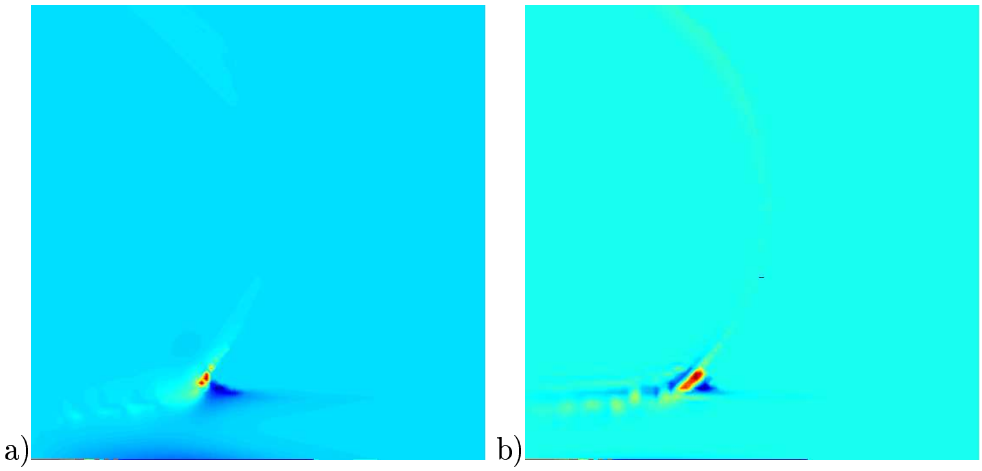

a) b)

Figure 12: Vorticity field near the neck of the impact for $t/\tau = 0.1$, $We = 8000$, and a) $Re = 100$ and b) $Re = 1000$. The color scale shows high vorticity region in dark. color

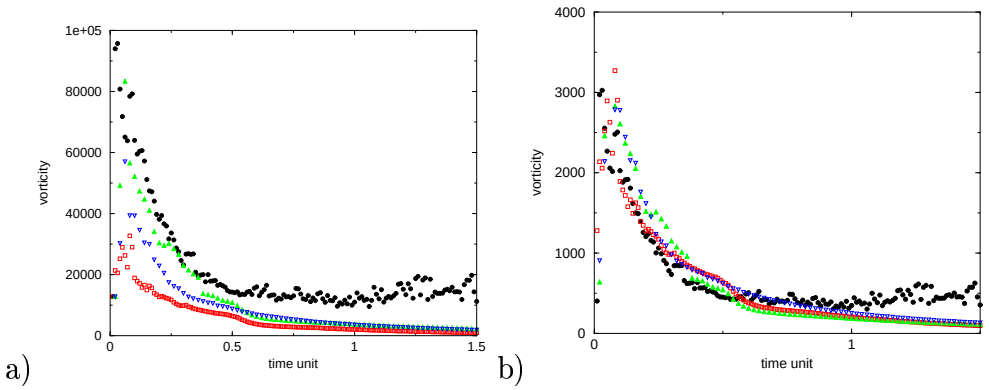

a) b)

Figure 13: a)Intensity of the vortex rings as a function of the time t/τ for $We = 8000$ and $Re = 100$, 200, 400 and 1000 (curves from bottom to top); b) same curves but where the vorticity is rescaled by $\sqrt{Re}$ so that the curves are now on the same scale.